



1 The instrument constant of sky radiometers (POM-02),

2 Part II: Solid view angle

3

4 Akihiro Uchiyama<sup>1</sup>, Tsuneo Matsunaga<sup>1</sup>, Akihiro Yamazaki<sup>2</sup>

5

6 <sup>1</sup> Center for Global Environmental Research, National Institute for Environmental

7 Studies, Tsukuba, Ibaraki, 305-8506, Japan

8 <sup>2</sup> Meteorological Research Institute, Japan Meteorological Agency, Tsukuba, Ibaraki,

9 305-0052, Japan

10 *Corresponding to:* Uchiyama Akihiro ([uchiyama.akihiro@nies.go.jp](mailto:uchiyama.akihiro@nies.go.jp))

11

12

13 **Abstract**

14 Ground-based networks have been developed to determine the spatiotemporal  
15 distribution of aerosols using sky radiometers. In this study, errors related to the solid  
16 view angle (SVA) of sky radiometers, which are used by SKYNET, were investigated.  
17 The SVA is calculated using solar disk scan data, the measured radiances around the  
18 solar direction in  $0.1 \times 0.1$  degree increments. These measurements include the  
19 scattered light from aerosol and air molecules, as well as the direct solar irradiance,  
20 causing errors in the SVA calculation. The influence of these errors was evaluated with  
21 simulations. From the results of these simulations, if the aerosol optical thickness is  
22 less than 0.5 at 550 nm and the aerosol does not include large particles, such as desert  
23 dust particles, then its influence on the SVA calculation was less than 0.5%. Problems  
24 with the software for the SVA calculation were also investigated. First, the data  
25 processing does not consider the change of airmass (solar zenith angle) during the  
26 solar disk scan measurement. In practice, if a measurement is made in the period  
27 when the change in airmass is small, then the error is small. Second, before starting  
28 data processing, the minimum measured value is subtracted from the measured values,  
29 resulting in underestimation of the SVA by 1 to 4%. Thirdly, the values between 1.4  
30 and 2.5 degrees are not properly extrapolated, resulting in overestimation of the SVA



31 by 0.6 to 2.1%. The second and third error sources partially cancel each other out, and  
32 the total error is an underestimation of 0.5 to 1.9% of the actual value. Furthermore,  
33 the annual trend in the SVA was examined. In both the visible and near-infrared  
34 regions, this trend cannot be seen in 4 and 8 years of data, respectively. The seasonal  
35 variation of the SVA was also examined, but no clear seasonal variation could be  
36 detected.

37

38

### 39 **1. Introduction**

40 Atmospheric aerosols are an important constituent of the atmosphere. Aerosols  
41 affect not only the global climate through the radiation budget both directly and  
42 indirectly (e.g., Ramanathan et al. 2001, Lohmann and Feichter 2005) but also human  
43 health as one of the main components of air pollution.

44 Atmospheric aerosols have a large variability in time and space. To measure the  
45 spatio-temporal distribution of aerosols, ground-based observation networks such as  
46 AERONET (AERosol ROBotic NETwork) (Holben et al. 1998) and SKYNET (Takamura  
47 and Nakajima 2004) have been developed and extended, and remote sensing methods  
48 from space have been developed using the near-ultraviolet to near-infrared  
49 wavelengths.

50 For ground-based observations, the solar direct irradiance and sky radiances are  
51 measured, and the aerosol characteristics are retrieved by analyzing these data. To  
52 improve the measurement accuracy, it is important to know the characteristics of the  
53 instrument and to be able to accurately calibrate it.

54 In SKYNET, radiometers POM-01 and POM-02 manufactured by Prede Co. Ltd.,  
55 Japan are used. These radiometers are called ‘sky radiometers’, and measure both the  
56 solar direct irradiance and sky radiances. The objectives in this study are to  
57 investigate the current status and issues with sky radiometers.

58 There are two constants that we must determine to be able to make accurate  
59 measurements. One is the calibration constant. The other is the solid view angle (SVA)  
60 of the radiometer. In Part I (Uchiyama et al. 201#), the temperature dependence of the  
61 sensor output was investigated and the calibration constants determined by the  
62 Improved Langley method and normal Langley method were compared. An alternative  
63 method to determine the calibration constant for the 940 nm channel and the  
64 near-infrared channels (1225, 1627, 2200 nm) was shown using on-site measurement  
65 data.

66 In Part II, the problem related to the SVA of the sky radiometer is described. The



67 SVA connects the sensor output to the sky radiance, which has units of  
68 energy/(wavelength)/sr. Overestimation (underestimation) in the SVA leads to  
69 underestimation (overestimation) of the single-scattering albedo (SSA). Therefore, it is  
70 necessary to accurately determine the SVA (Khatri et al. 2016, Hashimoto et al. 2012).

71 In section 2, the accuracy of the current method for the SVA calculation is  
72 investigated based on simulations. Then, in section 3, we describe the problem with the  
73 current SVA calculation program. This software is attached to the SKYRAD package  
74 (Nakajima et al. 1996), which is used to retrieve aerosol parameters from sky  
75 radiometer data. In section 4, we also show the trend in the SVA and seasonal  
76 variation using the data obtained at MLO and JMA/MRI. In section 5, the results and  
77 conclusions are presented.

78

## 79 **2. Simulation study of SVA estimation error**

80 The sensor output  $V$  when measuring the radiances from the sky with a sky  
81 radiometer can be written as follows:

$$82 \quad V = \int_{\Delta} C(\lambda_0) f(\Omega) I(\Omega) d\Omega \quad (1)$$
$$\quad = C(\lambda_0) \bar{I} \Delta\Omega$$

83 where  $C$  is the sensitivity,  $I(\Omega)$  is the sky radiance in the direction of  $\Omega$ ,  $f(\Omega)$  is  
84 the response function of the radiometer field of view,

$$85 \quad \bar{I} = \int_{\Delta} f(\Omega) I(\Omega) d\Omega / \Delta\Omega \quad (2)$$

$$86 \quad \Delta\Omega = \int_{\Delta} f(\Omega) d\Omega \quad (3)$$

87 and, for simplicity, the wavelength integration is omitted. Here,  $\Delta\Omega$  is the SVA,  
88 which is related to the mean sky radiance in the direction of  $\Omega$ , and errors in the SVA  
89 result in errors in the retrieved SSA. Therefore, the SVA is an important instrument  
90 parameter.

91 The SVA can be obtained by integrating the output of parallel light incident on the  
92 radiometer from all directions (see Appendix A). The SVA can also be obtained even if  
93 the light source has a finite size: the SVA can be obtained by integrating the output  
94 obtained while scanning the light source (see Appendix B).

95 To determine the SVA, a method using the measurement data around the sun was  
96 proposed by Nakajima et al. (1996). The radiances around the direction of the sun in  
97  $0.1 \times 0.1$  degree increments are measured; this is called a “solar disk scan”. Using  
98 these data, the SVA is calculated.



99 An example of measurements of the radiance of the sun and around the sun is shown  
 100 in Fig. 1. The measurement at POM-02 (red line) was performed horizontally at  
 101 intervals of 0.1 degree scattering angles, where the wavelength is 500 nm. Here,  
 102 “horizontally” means that the measurements were performed while keeping the zenith  
 103 angle the same as the solar zenith angle. In Fig. 1, the values measured by the image  
 104 sensor by shading the solar disk are also shown. Both measurement values are  
 105 normalized by the value at a scattering angle of  $-3$  degrees, where a negative value  
 106 means the left side is facing the sun. The image sensor can measure up to a scattering  
 107 angle of 1 degree. By comparing both measurements, we can see that the output of  
 108 POM-02 is affected by the direct solar irradiance for up to about 2.5 degrees from the  
 109 sun direction.

110 The hood of POM-02 is designed so that the full field of view (FOV) is 1 degree. The  
 111 size of the sun disk is about 0.5 degrees. Therefore, the direct solar irradiance can  
 112 enter the detector for angles up to about 0.75 degrees from the sun’s center. However,  
 113 the comparison between both measurements shows that the sensor output of POM-02  
 114 is affected by the direct solar irradiance for angles up to about 2.5 degrees from the  
 115 sun’s center.

116 The cause of the increase in the output is considered to be stray light. Since the  
 117 length of the hood and the size of the lens are finite, even if the angle from the sun  
 118 center exceeds 0.75 degrees, the direct solar light strikes the lens and results in “stray”  
 119 light. This stray light reaches the detector and increases the output, and is smaller  
 120 than the measurement of the direct sun by three orders of magnitude or more, but the  
 121 integrated value has a magnitude that can affect the estimation of the SVA.  
 122 Furthermore, when solar light is used as the light source, aerosols and air molecules  
 123 exist between the light source and the instrument. Therefore, the scattered light from  
 124 aerosols and air molecules is included in the measurement of the direct solar  
 125 irradiance. The influence of this scattered light must also be considered.

126 As seen from Fig. 1, roughly speaking, the FOV of POM-02 consists of a core part  
 127 from 0 to 0.5 degrees and a wing part from 0.5 to 2.5 degrees.

$$\begin{aligned}
 \Delta\Omega &= \Delta\Omega(\text{core}) + \Delta\Omega(\text{wing}) \\
 &= \int_{\Delta\Omega(\text{core})} f(\Omega)d\Omega + \int_{\Delta\Omega(\text{wing})} f(\Omega)d\Omega
 \end{aligned}
 \tag{3}$$

129 Estimating the magnitudes of the two terms gives the following:



$$\begin{aligned}
 \Delta\Omega(\text{core}) &= \int_{\Delta\Omega(\text{core})} f(\Omega) d\Omega \\
 &\cong \int_{\Delta\Omega(\text{core})} 1 \cdot d\Omega \\
 &= 2\pi(1 - \cos(0.5 \text{ deg})) \\
 &= 2.39 \times 10^{-4}
 \end{aligned} \tag{4}$$

$$\begin{aligned}
 \Delta\Omega(\text{wing}) &= \int_{\Delta\Omega(\text{wing})} f'(\Omega) d\Omega \\
 &\cong \int_{\Delta\Omega(\text{wing})} f_{\text{wing}} d\Omega \\
 &= 2\pi(\cos(0.5 \text{ deg}) - \cos(2.5 \text{ deg})) f_{\text{wing}} \\
 &= 5.74 \times 10^{-3} f_{\text{wing}}
 \end{aligned} \tag{5}$$

As seen from Fig. 1,  $f_{\text{wing}} \approx 10^{-3}$ . Therefore, the ratio of the terms is

$$\frac{\Delta\Omega(\text{wing})}{\Delta\Omega(\text{core})} \approx \frac{5.74 \times 10^{-3} f_{\text{wing}}}{2.39 \times 10^{-4}} = 2.4 \times 10^{-2} \tag{6}$$

This means that neglecting the wing part results in underestimation of the magnitude of the SVA by about 2%. If  $f_{\text{wing}} \approx 10^{-2}$ , then the contribution of the wing part to the SVA is about 20%, and the instrument should be repaired. If  $f_{\text{wing}} \approx 10^{-4}$ , then the contribution is about 0.2%, and the wing part can be ignored.

When the direction of the sun is measured, the sensor output  $V(\Omega = 0)$  is as follows:

$$\begin{aligned}
 V(\Omega = 0) &= C \left[ \int_{\Delta} f(\Omega') I_0 g(\Omega') d\Omega' + \int_{\Delta\Omega} I_{\text{sca}}(\Omega') f'(\Omega') d\Omega' \right] \\
 &= v(0) + C \Delta\Omega \bar{I}_{\text{sca}}(0)
 \end{aligned} \tag{7}$$

where

$$v(0) = C \int_{\Delta} f(\Omega') I_0 g(\Omega') d\Omega' \tag{8}$$

$$\bar{I}_{\text{sca}}(0) = \frac{1}{\Delta\Omega} \int_{\Delta\Omega} I_{\text{sca}}(\Omega') f'(\Omega') d\Omega' \tag{9}$$

and  $I_0 g(\Omega')$  is the solar radiance distribution. The first term on the right-hand side of eq. (7) is the contribution of the direct solar irradiance, and the second term is that of the scattered radiance.



146 When the direction of the sun is  $\Omega = \Omega_0$ , the sensor output  $V(\Omega = \Omega_0)$  is as  
 147 follows:

$$148 \quad V(\Omega = \Omega_0) = C \left[ \int_{\Delta} f(\Omega_0 + \Omega') I_0 g(\Omega') d\Omega' + \int_{\Delta\Omega} I_{sca}(\Omega_0 + \Omega') f(\Omega') d\Omega' \right] \quad (10)$$

$$= v(\Omega_0) + C\Delta\Omega \bar{I}_{sca}(\Omega_0)$$

149 where the first term on the right-hand side is the contribution of the direct solar  
 150 irradiance, and the second term is the scattered radiance. If  $\Omega_0$  is outside of the field  
 151 of view, then the first term is zero and only the second term is needed.

152 Currently, based on the data of the solar disk scan measurement, the SVA is  
 153 calculated by the following equation:

$$154 \quad \Delta\Omega' = \int_{\Delta\Omega} \frac{v(\Omega) + \Delta\Omega C \bar{I}_{sca}(\Omega)}{v(0) + \Delta\Omega C \bar{I}_{sca}(0)} d\Omega \quad (11)$$

155 If there is no scattered radiance, then

$$156 \quad \Delta\Omega' = \int_{\Delta\Omega} \frac{v(\Omega)}{v(0)} d\Omega \quad (12)$$

157 where  $\Delta\Omega'$  is the SVA  $\Delta\Omega$  (see Appendices A, B).

158 If the contribution of the scattered radiance is small, then  $\Delta\Omega' \cong \Delta\Omega$ . When the  
 159 optical thickness is large or the forward scattering is dominant, the contribution of the  
 160 scattered radiances increases.

161 We estimate the magnitude of each term of the integrand:

$$162 \quad \frac{v(\Omega) + \Delta\Omega C \bar{I}_{sca}(\Omega)}{v(0) + \Delta\Omega C \bar{I}_{sca}(0)} = \frac{v(\Omega) + \Delta\Omega C \bar{I}_{sca}(\Omega)}{v(0)(1 + \Delta\Omega C \bar{I}_{sca}(0)/v(0))} \quad (13)$$

163 Usually, the solar disk scan measurement is performed only when the scattered light is  
 164 much less than the direct solar irradiance:

$$165 \quad \Delta\Omega C \bar{I}_{sca}(0)/v(0) \ll 1.$$

166 The magnitude of this term has already been estimated from the influence of the  
 167 scattered radiance in the field of view in the measurement of the sun-photometer; the  
 168 estimation error of the optical thickness due to the scattered radiance in the field of  
 169 view (Zhao et al. 2012, Sinyuk et al. 2012).

170 Equation (13) can be approximated as follows:



$$\begin{aligned}
 \frac{v(\Omega) + \Delta\Omega \bar{C}I_{sca}(\Omega)}{v(0) + \Delta\Omega \bar{C}I_{sca}(0)} &\cong \frac{v(\Omega) + \Delta\Omega \bar{C}I_{sca}(\Omega)}{v(0)} \left(1 - \frac{\Delta\Omega \bar{C}I_{sca}(0)}{v(0)}\right) \\
 171 \quad &= \frac{v(\Omega) + \Delta\Omega \bar{C}I_{sca}(\Omega)}{v(0)} (1 - \varepsilon_3) \\
 &= \frac{v(\Omega)}{v(0)} + \frac{\Delta\Omega \bar{C}I_{sca}(\Omega)}{v(0)} - \frac{v(\Omega)}{v(0)} \varepsilon_3 - \frac{\Delta\Omega \bar{C}I_{sca}(\Omega)}{v(0)} \varepsilon_3
 \end{aligned} \tag{14}$$

172 where

$$173 \quad \varepsilon_3 = \frac{\Delta\Omega \bar{C}I_{sca}(0)}{v(0)}. \tag{15}$$

174 Therefore, eq. (11) is as follows.

$$\begin{aligned}
 \Delta\Omega' &= \int_{\Delta\Omega} \frac{v(\Omega) + \Delta\Omega \bar{C}I_{sca}(\Omega)}{v(0) + \Delta\Omega \bar{C}I_{sca}(0)} d\Omega \\
 175 \quad &\cong \Delta\Omega + \Delta\Omega \int_{\Delta\Omega} \frac{\bar{C}I_{sca}(\Omega)}{v(0)} d\Omega - \Delta\Omega \varepsilon_3 - \Delta\Omega \int_{\Delta\Omega} \frac{\bar{C}I_{sca}(\Omega)}{v(0)} d\Omega \varepsilon_3 \\
 &= \Delta\Omega \left\{ 1 + \int_{\Delta\Omega} \frac{\bar{C}I_{sca}(\Omega)}{v(0)} d\Omega - \varepsilon_3 - \varepsilon_3 \int_{\Delta\Omega} \frac{\bar{C}I_{sca}(\Omega)}{v(0)} d\Omega \right\}
 \end{aligned} \tag{16}$$

176 Since  $v(0) = CF_0$ , the above eq. (16) becomes

$$\begin{aligned}
 177 \quad \Delta\Omega' &\cong \Delta\Omega \left\{ 1 + \int_{\Delta\Omega} \frac{\bar{I}_{sca}(\Omega)}{F_0} d\Omega - \varepsilon_3 - \varepsilon_3 \int_{\Delta\Omega} \frac{\bar{I}_{sca}(\Omega)}{F_0} d\Omega \right\} \\
 &= \Delta\Omega \{ 1 + \varepsilon_2 - \varepsilon_3 - \varepsilon_2 \varepsilon_3 \}
 \end{aligned} \tag{17}$$

178 where

$$179 \quad \varepsilon_2 = \int_{\Delta\Omega} \frac{\bar{I}_{sca}(\Omega)}{F_0} d\Omega \tag{18}$$

180 The fourth term is smaller than the second and third terms and it can be ignored. Then,  
 181 comparing the second and third terms in the parenthesis,

$$182 \quad \varepsilon_2 = \int_{\Delta\Omega} \frac{\bar{I}_{sca}(\Omega)}{F_0} d\Omega = \int_{\Delta\Omega} \left\{ \frac{1}{F_0} \cdot \frac{1}{\Delta\Omega} \int_{\Delta\Omega} I_{sca}(\Omega + \Omega') f(\Omega') d\Omega' \right\} d\Omega \tag{19}$$

$$\begin{aligned}
 183 \quad \varepsilon_3 &= \frac{\Delta\Omega}{F_0} \cdot \frac{1}{\Delta\Omega} \int_{\Delta\Omega} I_{sca}(0 + \Omega') f(\Omega') d\Omega' \\
 &= \frac{\Delta\Omega \bar{I}_{sca}(\Omega = 0)}{F_0}
 \end{aligned} \tag{20}$$

184 where  $\varepsilon_2$  is the integral of the mean scattered light  $\bar{I}_{sca}(\Omega)$  in the region of



185  $f(\Omega) > 0$ , and  $\varepsilon_3$  is the integral of scattered light in the FOV when facing toward the  
 186 sun.

187 The  $f(\Omega)$  of the POM-02 consists of the core part from 0.0 to 0.5 degrees, which  
 188 takes large values, and the wing part from 0.5 to 2.5 degrees which takes small values.  
 189 Therefore, the integral can be written as follows.

$$190 \quad \varepsilon_2 = \int_{\Delta\Omega} \frac{\bar{I}_{sca}(\Omega)}{F_0} d\Omega = \int_{\Delta\Omega(core)} \frac{\bar{I}_{sca}(\Omega)}{F_0} d\Omega + \int_{\Delta\Omega(wing)} \frac{\bar{I}_{sca}(\Omega)}{F_0} d\Omega \quad (21)$$

191 Since  $\bar{I}_{sca}(\Omega) \approx \bar{I}_{sca}(\Omega = 0)$  in the core part,  $\int_{\Delta\Omega(wing)} f(\Omega) d\Omega \ll 1$ , and  $\int_{\Delta\Omega(core)} d\Omega \cong \Delta\Omega$ ,

192 the first term of the integral  $\varepsilon_2$  is as follows.

$$193 \quad \int_{\Delta\Omega(core)} \frac{\bar{I}_{sca}(\Omega)}{F_0} d\Omega \cong \frac{\bar{I}_{sca}(\Omega = 0)}{F_0} \Delta\Omega. \quad (22)$$

194 This means that the integral of the core part in the integral  $\varepsilon_2$  has the same  
 195 magnitude as  $\varepsilon_3$  and the two terms offset each other, whereas the integral of the wing  
 196 part remains. The area of the integral of the wing part is larger than that of the core  
 197 part. Even if the integral of scattered light in the FOV is small compared to the solar  
 198 direct irradiance, the integral of the wing part becomes large and introduces errors in  
 199 the SVA estimation. That is, even if the measurement value of scattered light is  
 200 smaller than the direct sun measurement,  $\bar{I}_{sca}(\Omega)\Delta\Omega/F_0 \approx 10^{-3}$ , the integral of the  
 201 wing part becomes large:

$$202 \quad \int_{\Delta\Omega(wing)} \frac{\bar{I}_{sca}(\Omega)}{F_0} d\Omega \approx \frac{\Delta\Omega(wing)}{\Delta\Omega} \times 10^{-3} \approx \frac{\Delta\Omega(wing)}{\Delta\Omega(core)} \times 10^{-3} = 2.4 \times 10^{-2}. \quad (23)$$

203 In this case, the magnitude of the error is about 2%.

204 Figures 2 and 3 show the values of  $\varepsilon_2$  and  $\varepsilon_3$  when the aerosol optical thickness  
 205 at 550 nm is changed. Here, the solar zenith angle is 30 degrees and the aerosol models  
 206 are the OPAC Continental average, Urban, and Desert types (Hess et al. 1998). The  
 207 simulation calculations of the scattered sky radiances were performed using the  
 208 subroutine in the SKYRAD package. The Ångström exponents of the Continental  
 209 average in the shorter (350 to 500 nm) and longer (500 to 800 nm) wavelength regions  
 210 are 1.11 and 1.42, respectively. Those of the Urban areas are 1.14 and 1.43, respectively,  
 211 and those of the Desert are 0.20 and 0.17, respectively.

212 When comparing  $\varepsilon_2$  and  $\varepsilon_3$ , the signs are opposite and partially cancel out.





213 However,  $\varepsilon_3$  is one order of magnitude smaller than  $\varepsilon_2$ , and thus  $\varepsilon_2$  contributes to  
214 the error in the calculation of the SVA. In the Continental average and Urban models,  
215 if the aerosol optical thickness at 550 nm is less than 0.5, the second term  $\varepsilon_2$  is less  
216 than 0.5%, and if the aerosol optical thickness at 550 nm is less than 1, the second  
217 term  $\varepsilon_2$  is less than 1%. In the Desert model, which includes large particles, the  
218 second term is less than 1% for shorter wavelengths, where desert particles have a  
219 higher absorption than in the longer wavelength regions. However, even if the aerosol  
220 optical thickness at 550 nm is less than 0.5, the second term is larger than 1% for some  
221 wavelengths.

222 From these simulations, if the scattered light can be removed from the SVA  
223 calculation, then an improvement in the accuracy of the calculations can be expected.  
224 However, since the intensity of the scattered light depends on aerosol characteristics, it  
225 is difficult to estimate the intensity of the scattered light from the measurements.  
226 Furthermore, close to the sun, the value of scattered light cannot be measured due to  
227 the direct sunlight. In POM-01 and POM-02, scattered light can only be measured  
228 without being affected by direct sunlight at scattering angles of more than 3 degrees.

229 The SVA was calculated by subtracting the measurements for a scattering angle of 3  
230 degrees and the accuracy of the estimation was examined. Although not shown in  
231 detail, for the continental average and urban models, even if the aerosol optical  
232 thickness is 2 at 550 nm, the error in the SVA estimation was less than 0.5%. This  
233 indicates that if the measured value of scattered light can be subtracted, the  
234 estimation accuracy of the SVA can be greatly improved.

235 From these results, when we determine the SVA by using the data from the solar  
236 disk scan measurement, if the aerosol optical thickness is less than 0.5 and the aerosol  
237 does not include large particles such as desert dust particles, the effect of the scattered  
238 radiances on the SVA calculation is less than 0.5%, and  $\Delta\Omega$  is well approximated by  
239  $\Delta\Omega'$ . Furthermore, if the measured value of the scattered light can be subtracted, the  
240 estimation accuracy of SVA can be greatly improved.

241

### 242 3. SVA calculation with the SKYRAD package

243 The software in the SKYRAD package is often used for SVA calculation from the data  
244 of the solar disk scan measurement. However, the authors noticed that there are  
245 problems in this program, and this section investigates these problems in detail.

246 In the measurement of the solar disk scan, a range of  $\pm 1$  degree in the zenith angle  
247 direction and  $\pm 1$  degree in the azimuth direction relative to the sun in increments of  
248 0.1 degrees is used, which produces a  $21 \times 21$  grid with angular resolution of 0.1



249 degrees. Therefore, the data are taken from the sun for scattering angles of up to about  
250  $1.4 (= (1 \text{ degree}) \times \sqrt{2})$  degrees. As shown in Fig. 1, the influence of the direct solar  
251 irradiance as a light source extends to about 2.5 degrees. To take this into  
252 consideration, the integration is performed by extrapolation for angles larger than 1.4  
253 degrees.

254 The following three problems exist in the SKYRAD package for calculating the SVA.

255 First, the data processing does not consider changes in the airmass (solar zenith  
256 angle) during the solar disk scan measurement. However, in practice, if the solar disk  
257 scan measurement is conducted when the airmass change (solar zenith angle) is small,  
258 then the resulting error is also small. Also, this is not usually a problem unless the  
259 measurement is conducted over an extended period of time.

260 Second, before starting the data processing, the minimum measured value is  
261 subtracted from the measured values. As a result, the measurements of the scattering  
262 angle between 1 and 1.4 degrees are greatly affected. By integrating the measured  
263 value minus the minimum, the SVA is always underestimated, but the solution to this  
264 problem is not straightforward.

265 Thirdly, the values between 1.4 and 2.5 degrees are not properly extrapolated.  
266 Frequently, the extrapolated value does not decrease monotonically. In some cases, this  
267 partially cancels out the underestimation of the integral.

268 In Fig. 4, an example of the integrand for the SVA calculation is shown. In the blue  
269 curve with open squares, the minimum value is subtracted. This curve is then  
270 integrated by the current SKYRAD program. Since the minimum value is subtracted,  
271 the difference is noticeable at scattering angles greater than 1 degree. In this case, the  
272 extrapolated value from 1.4 to 2.5 degrees is almost constant. In many cases, nearly  
273 constant values were extrapolated as in this example. In some cases, the extrapolated  
274 values increased. In the red curve with open circles, the minimum value is not  
275 subtracted. The values between 1.4 and 2.5 degrees were extrapolated using the data  
276 from 1.0 to 1.4 degrees. Considering Fig. 1, the decreasing trend is more realistic.

277 To investigate the differences in the calculation methods, several calculations were  
278 performed.

279 The following steps in the calculations were varied,

- 280 (1) Whether the minimum value was subtracted.
- 281 (2) Whether the change in airmass was considered.
- 282 (3) The method for the extrapolation in the range from 1.4 to 2.5 degrees.
- 283 (4) Whether the horizontal cross-section of the FOV is assumed to be a circle or an



284 ellipse (the current SKYRAD package method uses an ellipse).

285 (5) The method for determining the ellipse's parameters.

286 Data taken at MLO in October and November in 2015 were used in this study.

287 The solar disk scan measurement was made between 10:00 and 13:00 local time at  
288 MLO. The optical thicknesses at wavelengths of 500 and 340 nm were at most 0.1 and  
289 0.5, respectively. Therefore, the influence of the scattered light on the SVA calculation  
290 is small.

291 The SAV was calculated for the six cases shown in Table 1, including Case 1, which is  
292 the current method used by the SKYRAD package. In Cases 4, 5, and 6, the values in  
293 the range 1.4 to 2.5 degrees were extrapolated as a linear function of the cosine of the  
294 scattering angle. This linear function was determined by the least squares method  
295 using the data with a scattering angle of more than 1 degree. The elliptic parameters  
296 in Case 6 were determined by assuming that the shape of the FOV is a 2-dimensional  
297 Gaussian distribution. The results of the comparison are summarized in Table 2.

298 The difference between Case 1 and Case 2 is whether or not the minimum value was  
299 subtracted. Case 1, in which the minimum value was subtracted, results in an  
300 underestimation of about 1 to 4%.

301 The difference between Case 2 and Case 3 is whether the change in airmass was  
302 considered or not. The solar disk scan measurement was made between 10:00 and  
303 13:00 local time at MLO. Therefore, the change in the air mass is less than 0.01, and  
304 there was hardly any influence from the change in airmass.

305 The difference between Case 3 and Case 4 is the method of extrapolation used in the  
306 range from 1.4 to 2.5 degrees. In the current SKYRAD package, the SVA was  
307 overestimated by 0.6 to 2.1%.

308 Since there was hardly any influence from the change in airmass, in Case 1 and Case  
309 4 the underestimation caused by the subtraction of the minimum value and the  
310 overestimation caused by the poor extrapolation partially cancel each other out, and  
311 the current SKYRAD package method underestimates the SVA by 0.5 to 1.9%.

312 The difference between Case 3 and Case 5 is whether the horizontal cross-section of  
313 the FOV is assumed to be a circle or an ellipse. The difference between them was less  
314 than 0.1%. This indicates that POM-02 was well tuned when it was shipped from the  
315 manufacturer.

316 In Case 6, a different method for determining elliptic parameters from the current  
317 SKYRAD package was used. Therefore, the difference between Case 4 and Case 6 is  
318 the difference between the methods used to determine the elliptic parameters. There  
319 was almost no difference between the current method and the new method. The



320 method used to determine the elliptic parameters thus has little effect on the SVA  
321 estimation.

322

#### 323 **4. Annual trend and seasonal variation of SVA**

324 Broadly speaking, the SVA is determined by the size of the pinhole and the focal  
325 length of the lens. There is a possibility that these parameters may change with  
326 degradation and the inside temperature. Therefore, the annual trend and seasonal  
327 variation of the SVA are examined.

328 Figures 5 and 6 show the SVAs in the visible region (Si photodiode) and in the  
329 near-infrared region (InGaAs photodiode) from 2008 and 2016, respectively. The  
330 observation for the calibration at MLO was performed over about a month in October  
331 and November every year. The lens in the visible region was replaced before the  
332 observation in 2013.

333 In Fig. 5(a), time series of the SVA in channels 1 to 8 are shown for the SVA  
334 calculated by the corrected method in this study. In Fig. 5(b), the SVA in channel 4 (500  
335 nm) calculated by both the corrected and the current SKYRAD package methods are  
336 shown for comparison. As stated in the above section, the SVA calculated by the  
337 current method is lower than that calculated by the corrected one except for 2008.  
338 Since the lens in the visible region was replaced before the calibration observation in  
339 2013, it is difficult to investigate the annual trend of the SVA. Additionally, from this  
340 figure, the accuracy of the SVA ((standard deviation)/mean) is estimated at about 1%  
341 except in 2015.

342 From 2008 to 2012, the value of the SVA seems to be decreasing. The value of the  
343 SVA in 2008 is larger than in other years. The values of the SVA are within  $\pm 0.5\%$   
344 except in 2008. From 2013 to 2016, the values of the SVA are within  $\pm 1\%$ . The annual  
345 variation of the SVA is less than or equal to the accuracy of the SVA. From these  
346 results, the annual trend in the SVA cannot be seen in only 4 years of data, and even if  
347 there is a trend, it is smaller than the measurement accuracy.

348 Figure 6(a) is the same as Fig. 5(a) except for channels 9 to 11 (1225, 1627, 2200 nm)  
349 and Fig. 6(b) is the same as Fig. 5(b) except for channel 10 (1627 nm). In these  
350 channels, the SVA calculated by the current method is also lower than that calculated  
351 by the corrected one except in 2008.

352 The determination accuracy of the SVA is also estimated as about 1%. The lens in the  
353 near-infrared region was not replaced in the period from 2008 to 2016. The trend in the  
354 SVA cannot be seen in 8 years of data either. The values of the SVA in this period are  
355 within  $\pm 1\%$ , which is the determination accuracy of the SVA. From these results, the



356 annual trend of the SVA in the near-infrared channels cannot be seen in 8 years of data,  
357 and even if there is a trend, it is smaller than the measurement accuracy.

358 Figure 7 shows the SVAs of POM-02 (Tsukuba) in the 500 and 1627 nm channels in  
359 the period from January 2014 to December 2016. All data are plotted and the data are  
360 scattered about  $\pm 2\%$ , though the values in 2014 are a bit low. There is a large amount  
361 of data in the winter, because there are many fine days in the winter in Tsukuba.  
362 There are little data from spring to autumn and the data in the summer are scattered.  
363 Since the estimated SVA is scattered, it is not possible to draw a clear conclusion, but  
364 as can be seen from Fig. 7, the seasonal variation exceeding  $\pm 2\%$  cannot be confirmed  
365 in either channel. This also indicates that the temperature dependence of the SVA in  
366 both detector regions cannot be seen. Since the data are taken over a short period of 3  
367 years, no annual trend in the SVA can be detected.

368

## 369 5. Summary and conclusion

370 Atmospheric aerosols are an important constituent of the atmosphere. Measurement  
371 networks covering an extensive area from ground and space have been developed.  
372 SKYNET is a ground-based monitoring system using sky radiometers POM-01 and  
373 POM-02 (Prede Co. Ltd., Japan). To improve the measurement accuracy, it is  
374 important to know the characteristics of the instruments and calibrate them. There  
375 are two constants that we must determine to make accurate measurements. One is the  
376 calibration constant, and the other is the SVA of the radiometer.

377 In Part I, problems related to the estimation of the calibration constant were  
378 investigated, and in Part II, problems related to the determination of the SVA of the  
379 sky radiometer were described.

380 In this study, the data from two sky radiometers POM-02 of the JMA/MRI are  
381 analyzed. One of the sky radiometers is used as a calibration reference, and the other  
382 is used for the continuous measurement at the Tsukuba MRI observation site.

383 The FOV of POM-02 consists of a core part from 0 to 0.5 degrees and a wing part  
384 from 0.5 to 2.5 degrees. The wing part is about 3 orders of magnitude smaller than the  
385 core part, but the wing part contributes about 2% to the SVA.

386 A method for determining the SVA using the sun as a light source was proposed by  
387 Nakajima et al. (1996). In this method, the radiance around the direction of the sun in  
388  $0.1 \times 0.1$  degree increments is measured. These measurements include the scattered  
389 light from aerosols and air molecules as well as the direct solar irradiance. These  
390 scattered radiances cause errors in the SVA calculation.

391 The influence of the scattered light was evaluated by simulations. As a result, if the



392 aerosol optical thickness is less than 0.5 at a wavelength of 550 nm and the aerosol  
393 does not include large particles such as desert dust particles, then the effect of the  
394 scattered radiances on the SVA calculation is less than 0.5%. Furthermore, if the  
395 measurements of the scattered light can be taken into account, the estimation accuracy  
396 of SVA can be greatly improved.

397 The SKYRAD package for determining the SVA from the solar disk scan  
398 measurements has several problems. The problems do not result in major errors in the  
399 estimation of the SVA, but can cause a systematic underestimation.

400 First, the data processing does not consider the change in the airmass (solar zenith  
401 angle) during the solar disk scan measurement. In practice, if the measurements are  
402 taken over a period when the change in airmass is small, then there is almost no  
403 problem. Second, before beginning the data processing, the minimum value is  
404 subtracted from each measured value. This results in an underestimation of the SVA  
405 by 1 to 4%. Thirdly, the values between 1.4 and 2.5 degrees are not properly  
406 extrapolated. This overestimates the SVA value by 0.6 to 2.1%. Since the second and  
407 third errors partially cancel each other out, if the current software is used, the error  
408 will finally be an underestimation by 0.5 to 1.9%.

409 The annual trend in the SVA was examined using the data taken at MLO. Since the  
410 optical thickness at a wavelength of 500 nm is 0.1 at most at MLO, the influence of the  
411 scattered light is small. The accuracy of the SVA was estimated as about 1%. In the  
412 visible region, the annual trend in the SVA cannot be seen in only 4 years of data from  
413 2009 to 2012 and 2013 to 2016, and it is smaller than the measurement accuracy. In  
414 the near-infrared region, the annual trend of the SVA cannot be seen in 8 years data  
415 from 2008 to 2016, and it is smaller than the measurement accuracy.

416 The seasonal variation of the SVA was examined using the data taken at Tsukuba  
417 from January 2014 to December 2016. Since the time series of the determined SVA was  
418 scattered  $\pm 2\%$ , it is not possible to draw a clear conclusion, but seasonal variation  
419 exceeding  $\pm 2\%$  could not be confirmed. Furthermore, as the temporal range of the data  
420 was short, no annual trend could be detected.

421

#### 422 **Acknowledgements**

423 This work was supported by the NIES GOSAT-2 project, Japan. This work was also  
424 partially supported by JSPS KAKENHI Grant Number JP17K00531.

425

426

#### 427 **Appendix A**



428 Let  $f(\Omega)$  be the response function of the FOV, where  $\Omega$  indicates the direction,  
 429 and when  $\Omega = 0$ ,  $f(\Omega = 0) = 1$ .

430 The SVA is then as follows:

$$431 \quad \Delta\Omega = \int_{\Delta} f(\Omega)d\Omega. \quad (\text{A1})$$

432 Suppose parallel light enters from  $\Omega = \Omega_0$ .

$$433 \quad \begin{aligned} V(\Omega = \Omega_0) \\ &= C \int_{\Delta} f(\Omega)\delta(\Omega - \Omega_0)F_0d\Omega \\ &= Cf(\Omega = \Omega_0)F_0 \end{aligned} \quad (\text{A2})$$

434 Therefore,

$$435 \quad f(\Omega_0) = \frac{V(\Omega_0)}{CF_0}. \quad (\text{A3})$$

436 Since  $f(0) = 1$ , then  $V(0) = CF_0$ .

437 Therefore,

$$438 \quad \begin{aligned} \Delta\Omega &= \int_{\Delta} f(\Omega)d\Omega \\ &= \int_{\Delta} \frac{V(\Omega_0)}{CF_0}d\Omega_0 \\ &= \int_{\Delta} \frac{V(\Omega_0)}{V(0)}d\Omega_0 \end{aligned} \quad (\text{A4})$$

439 When the parallel light is incident, the SVA of the radiometer can be obtained by  
 440 integrating the output in an arbitrary direction normalized by the output in the  
 441 direction of  $\Omega = 0$ .

442

#### 443 **Appendix B**

444 Here, we consider the case that the light source has a finite size, for example, when  
 445 the sun is used as a light source.

446 Let the radiance distribution of the light source be  $I(\Omega) = I_0g(\Omega)$ .

447 The integrated energy of the light source  $F_0$  is as follows,

$$448 \quad F_0 = \int_{\Delta} g(\Omega)I_0d\Omega \quad (\text{B1})$$

449 where  $\Delta$  is the extent of the light source.

450 Considering the sun as a light source, let  $\Delta$  be smaller than  $\Delta\Omega$ . Also, when the  
 451 sun is a light source,  $F_0$  is the solar irradiance.

452 Let  $C$  be the sensitivity of the detector, where  $C$  is the proportional constant of



453 the sensor output and input energy.

454 The light source is in the direction of  $\Omega = 0$  and we measure the radiance from it as

$$\begin{aligned}
 v(0) &= C \int_{\Delta} f(0 + \Omega') g(\Omega') I_0 d\Omega' \\
 &= CI_0 \int_{\Delta} f(\Omega') g(\Omega') d\Omega'
 \end{aligned} \tag{B2}$$

456 where  $v(0)$  is the sensor output.

457 If  $f(\Omega)$  is constant within the range of  $\Delta$  (POM-02 satisfies this condition), then  
 458 this equation can be rewritten as follows:

$$\begin{aligned}
 v(0) &= CI_0 \int_{\Delta} f(\Omega') g(\Omega') d\Omega' \\
 &= CI_0 f(0) \int_{\Delta} g(\Omega') d\Omega' \\
 &= Cf(0)F_0 \\
 &= CF_0
 \end{aligned} \tag{B3}$$

460 Next, the light source is in the direction of  $\Omega = \Omega_0$ ,

$$v(\Omega_0) = CI_0 \int_{\Delta} f(\Omega_0 + \Omega') g(\Omega') d\Omega' \tag{B4}$$

462 where  $v(\Omega_0)$  is the sensor output.

463 Then, both sides of the equation are integrated within the SVA  $\Delta\Omega$ ,

$$\int_{\Delta\Omega} v(\Omega_0) d\Omega_0 = \int_{\Delta\Omega} \left( CI_0 \int_{\Delta} f(\Omega_0 + \Omega') g(\Omega') d\Omega' \right) d\Omega_0 \tag{B5}$$

465 By changing the order of integration on the right, the following equation can be  
 466 obtained:

$$\begin{aligned}
 \int_{\Delta\Omega} v(\Omega_0) d\Omega_0 &= CI_0 \int_{\Delta} \left( g(\Omega') \int_{\Delta\Omega} f(\Omega_0 + \Omega') d\Omega_0 \right) d\Omega' \\
 &= CI_0 \int_{\Delta} g(\Omega') d\Omega' \cdot \Delta\Omega \\
 &= CF_0 \Delta\Omega
 \end{aligned} \tag{B6}$$

468 Therefore, from eqs. (B3) and (B6),

$$\begin{aligned}
 \Delta\Omega &= \frac{1}{CF_0} \int_{\Delta\Omega} v(\Omega_0) d\Omega_0 \\
 &= \int_{\Delta\Omega} \frac{v(\Omega_0)}{v(0)} d\Omega_0
 \end{aligned} \tag{B7}$$

470 Thus, even in the case that the light source has a finite size, the SVA of the





471 radiometer can be obtained in the same manner as in the case of the parallel light  
472 source.

473

474

#### 475 **References**

476 Hashimoto M., T. Nakajima, O. Dubovik, M. Campanelli, H. Che, P. Khatri, T.  
477 Takamura, and G. Pandithurai, 2012: Development of a new data-processing method  
478 for SKYNET sky radiometer observations, *Atmos. Meas. Tech.*, **5**, 2723–2737, 2012,  
479 [www.atmos-meas-tech.net/5/2723/2012/doi:10.5194/amt-5-2723-2012](http://www.atmos-meas-tech.net/5/2723/2012/doi:10.5194/amt-5-2723-2012)

480 Hess, M., P. Koepke, and I. Schult, Optical Properties of Aerosols and Clouds, 1998:  
481 The Software Package OPAC. *Bull. Am. Meteorol. Soc.*, **79**, 5, 831–844.

482 Holben, B. N., T. F. Eck, I. Slutsker, D. Tanré, J. P. Buis, A. Setzer, E. Vermote, J. A.  
483 Reagan, Y. J. Kaufman, T. Nakajima, F. Lavenu, I. Jankowiak, and A. Smirnov, 1998:  
484 AERONET-A federated instrument network and data archive for aerosol  
485 characterization. *Remote Sens. Environ.*, **66**, 1–16.

486 P. Khatri, P., T. Takamura, T. Nakajima, V. Estellés, H. Irie, H. Kuze, M. Campanelli, A.  
487 Sinyuk, S.-M. Lee, B. J. Sohn, G. Pandithurai, S.-W. Kim, S. C. Yoon, J. A.  
488 Martinez-Lozano, M. Hashimoto, P. C. S. Devara, and N. Manago, 2016: Factors for  
489 inconsistent aerosol single scattering albedo between SKYNET and AERONET, *J.*  
490 *Geophys. Res. Atmos.*, **121**, 1859–1877, doi:10.1002/2015JD023976.

491 Lohmann, U., and J. Feichter, 2005: Global indirect aerosol effects: a review. *Atmos.*  
492 *Chem. Phys.*, **5**, 715–737.

493 Nakajima, T., G. Tonna, R. Rao, Y. Kaufman, and B. Holben, 1996: Use of sky  
494 brightness measurements from ground for remote sensing of particulate  
495 polydispersions, *Appl. Opt.*, **35**, 2672–2686.

496 Ramanathan, V., P. J. Crutzen, J. T. Kiehl, and D. Rosenfeld, 2001: Aerosols, Climate,  
497 and the Hydrological Cycle. *Science*, **294**, 2119–2124.

498 Sinyuk, A., B. N. Holben, A. Smirnov, T. F. Eck, I. Slutsker, J. S. Schafer, D. M. Giles,  
499 and M. Sorokin, 2012: Assessment of error in aerosol optical depth measured by  
500 AERONET due to aerosol forward scattering, *Geophys. Res. Lett.*, **39**, L23806,  
501 doi:10.1029/2012GL053894.

502 Takamura, T., T. Nakajima and SKYNET community group, 2004: Overview of  
503 SKYNET and its Activities. Proceedings of AERONET workshop. *El Arenosillo.*  
504 *Optica Pura y Aplicada*, **37**, 3303–3308.

505 Uchiyama A., T. Matsunaga and A. Yamazki, 2017: The instrument constant of sky  
506 radiometers (POM-02), Part I; Calibration constant, *Atmos. Meas. Tech.* (to be



507 submitted)

508 Zhao, F., Y. Tan, Z. Li, and C. Gai ,2012: The effect and correction of aerosol forward

509 scattering on retrieval of aerosol optical depth from Sun photometer measurements,

510 *Geophys. Res. Lett.*, **39**, L14805, doi:10.1029/2012GL052135.

511



512 Table titles

513 Table 1 Settings of the SVA calculation

514

515 Table 2 Influence of the different calculation settings.

516 (a) Calculated SVA. The data taken at MLO in October and November 2015 are used.

517 (b) Comparison of calculated SVA.

518

519 Figure captions

520 Fig. 1 Example of the measurement of the sun and the sky around the sun.

521 The measurement was performed keeping the same zenith angle as the solar zenith

522 angle. A negative (positive) scattering angle means the left (right) side of the

523 instrument is facing the sun. The red line with an open circle is the output of POM-02,

524 and the blue line is the output of the image sensor when shading the solar disk. Both

525 outputs are normalized by the value at a scattering angle of  $-3$  degrees.

526

527 Fig. 2 Estimation of the error  $\varepsilon_2$  in the calculation of the SVA. Aerosol models are the

528 OPAC Continental average, Urban, and Desert. The aerosol optical thickness is that at

529 a wavelength of 550 nm and the solar zenith angle is 30 degrees.

530

531 Fig. 3 Same as Fig. 2 but for error  $\varepsilon_3$ .

532

533 Fig. 4 Example of the integrand of the SVA calculation. The blue line with open

534 squares is for the case that the minimum value is subtracted, and the red line is for the

535 case that the values between 1.4 and 2.5 degrees are extrapolated using the data from

536 1.0 to 1.4 degrees.

537

538 Fig. 5 SVAs in the visible region (Si photodiode) from 2008 to 2016. The data were

539 taken at MLO over a month in October and November every year. (a) SVA calculated by

540 the corrected method in this study, (b) SVA at a wavelength of 500 nm calculated by

541 both the corrected and the current SKYRAD package methods.

542

543 Fig. 6 Same as Fig. 5 but for the near-infrared region (InGaAs photodiode). The

544 wavelength in (b) is 1627 nm.

545

546 Fig. 7 Time series of the SVA at POM-02 (Tsukuba) from January 2014 to December

547 2016: (a) 500 nm, (b) 1627 nm.

548



549

550 Table 1 Settings of the SVA calculation.

	subtract minimum value	consideration of airmass change	extrapolation method	FOV shape
case 1	yes	no	current	elliptic
case 2	no	no	current	elliptic
case 3	no	yes	current	elliptic
case 4	no	yes	new	elliptic
case 5	no	yes	current	circular
case 6	no	yes	new	elliptic

551 Case 1 is the method implemented in the current SKYRAD package.

552 The elliptic shape parameters in Case 6 are calculated by a different method from the

553 SKYRAD package.

554



Table 2 Influence of the different calculation settings.

(a) Calculated SVA. The data taken at MLO in October and November 2015 are used.

WLN (nm)		340	380	400	500	675	870	940	1020	1225	1627	2200
Case_1 (C1)	SVA( $\times 10^{-4}$ )	2.4495	2.4643	2.4472	2.4366	2.4530	2.4404	2.4554	2.4567	2.0086	2.0152	2.0692
	SD( $\times 10^{-4}$ )	0.0379	0.0407	0.0403	0.0388	0.0374	0.0277	0.0296	0.0241	0.0287	0.0241	0.0214
	SD/SVA	0.0155	0.0165	0.0165	0.0159	0.0153	0.0113	0.0121	0.0098	0.0143	0.0120	0.0103
Case_2 (C2)	SVA( $\times 10^{-4}$ )	2.5014	2.5186	2.5036	2.4764	2.4782	2.4995	2.5322	2.5564	2.0586	2.0737	2.1328
	SD( $\times 10^{-4}$ )	0.1151	0.1116	0.1144	0.0838	0.0579	0.0346	0.0314	0.0257	0.0294	0.0260	0.0233
	SD/SVA	0.0460	0.0443	0.0457	0.0338	0.0234	0.0138	0.0124	0.0101	0.0143	0.0125	0.0109
Case_3 (C3)	SVA( $\times 10^{-4}$ )	2.5015	2.5184	2.5035	2.4765	2.4783	2.4993	2.5320	2.5565	2.0586	2.0737	2.1327
	SD( $\times 10^{-4}$ )	0.1151	0.1115	0.1144	0.0838	0.0580	0.0344	0.0315	0.0258	0.0295	0.0260	0.0233
	SD/SVA	0.0460	0.0443	0.0457	0.0338	0.0234	0.0138	0.0124	0.0101	0.0143	0.0125	0.0109
Case_4 (C4)	SVA( $\times 10^{-4}$ )	2.4693	2.4899	2.4698	2.4534	2.4641	2.4691	2.4923	2.5023	2.0346	2.0440	2.1005
	SD( $\times 10^{-4}$ )	0.0668	0.0804	0.0698	0.0580	0.0459	0.0304	0.0302	0.0259	0.0301	0.0259	0.0227
	SD/SVA	0.0271	0.0323	0.0283	0.0236	0.0186	0.0123	0.0121	0.0104	0.0148	0.0127	0.0108
Case_5 (C5)	SVA( $\times 10^{-4}$ )	2.5027	2.5199	2.5032	2.4777	2.4783	2.5010	2.5329	2.5565	2.0596	2.0750	2.1336
	SD( $\times 10^{-4}$ )	0.1155	0.1123	0.1141	0.0831	0.0583	0.0346	0.0312	0.0262	0.0298	0.0261	0.0236
	SD/SVA	0.0461	0.0446	0.0456	0.0335	0.0235	0.0138	0.0123	0.0102	0.0145	0.0126	0.0111
Case_6 (C6)	SVA( $\times 10^{-4}$ )	2.4694	2.5042	2.4698	2.4535	2.4637	2.4698	2.4921	2.5028	2.0349	2.0449	2.1014
	SD( $\times 10^{-4}$ )	0.0669	0.1249	0.0701	0.0576	0.0463	0.0297	0.0305	0.0264	0.0312	0.0258	0.0225
	SD/SVA	0.0271	0.0499	0.0284	0.0235	0.0188	0.0120	0.0122	0.0106	0.0153	0.0126	0.0107



(b) Comparison of calculated SVA.

WLN (nm)	340	380	400	500	675	870	940	1020	1225	1627	2200	
C2/C1-1	0.0212	0.0220	0.0230	0.0163	0.0103	0.0242	0.0313	0.0406	0.0249	0.0290	0.0307	min. value subtraction
C3/C2-1	0.0000	-0.0001	0.0000	0.0000	0.0000	-0.0001	-0.0001	0.0000	0.0000	0.0000	0.0000	airmass change
C4/C3-1	-0.0129	-0.0113	-0.0135	-0.0093	-0.0057	-0.0121	-0.0157	-0.0212	-0.0117	-0.0143	-0.0151	different extrapolation
C4/C1-1	0.0081	0.0104	0.0092	0.0069	0.0045	0.0118	0.0150	0.0186	0.0129	0.0143	0.0151	min. value subtraction, different extrapolation
C5/C3-1	0.0005	0.0006	-0.0001	0.0005	0.0000	0.0007	0.0004	0.0000	0.0005	0.0006	0.0004	circular or elliptic shape
C6/C4-1	0.0000	0.0057	0.0000	0.0000	-0.0002	0.0003	-0.0001	0.0002	0.0001	0.0004	0.0004	different elliptic parameters



Fig.1

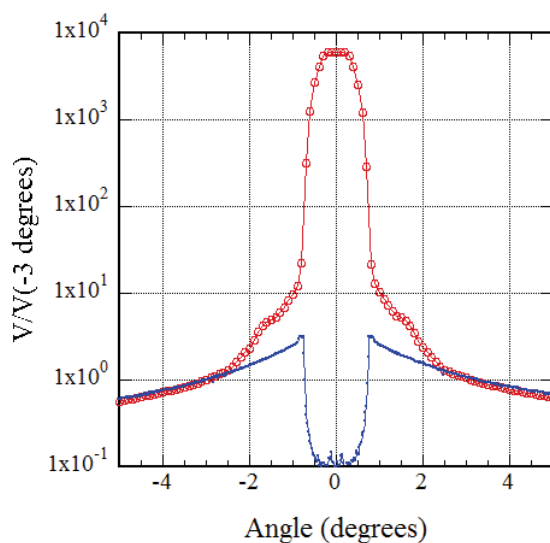


Fig. 1 An example of measurement of the sun and the sky around the sun. The measurement was performed keeping the same zenith angle as the solar zenith angle. A negative (positive) scattering angle means the left (right) side facing the sun. The red line with open circle is output of POM-02, and the blue line is output of image sensor output by shading the solar disk. Both output are normalized by the value at scattering angle -3 degrees



Fig. 2

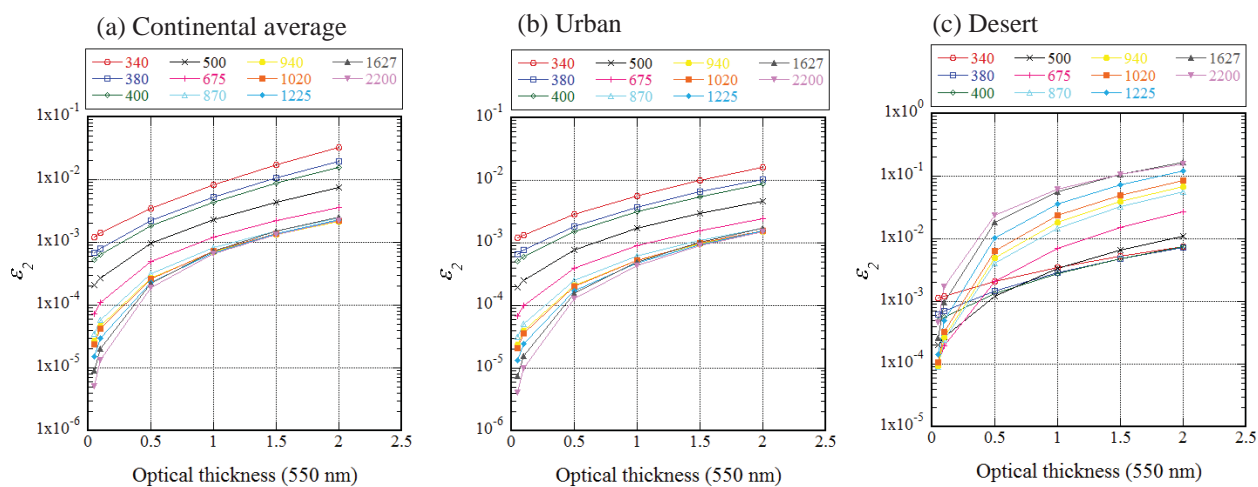


Fig. 2 Estimation of error  $\varepsilon_2$  in calculation of SVA. Aerosol models are OPAC continental average, urban and desert. The aerosol optical thickness is that at the wavelength of 550nm and the solar zenith angle is 30 deg.





Fig. 3

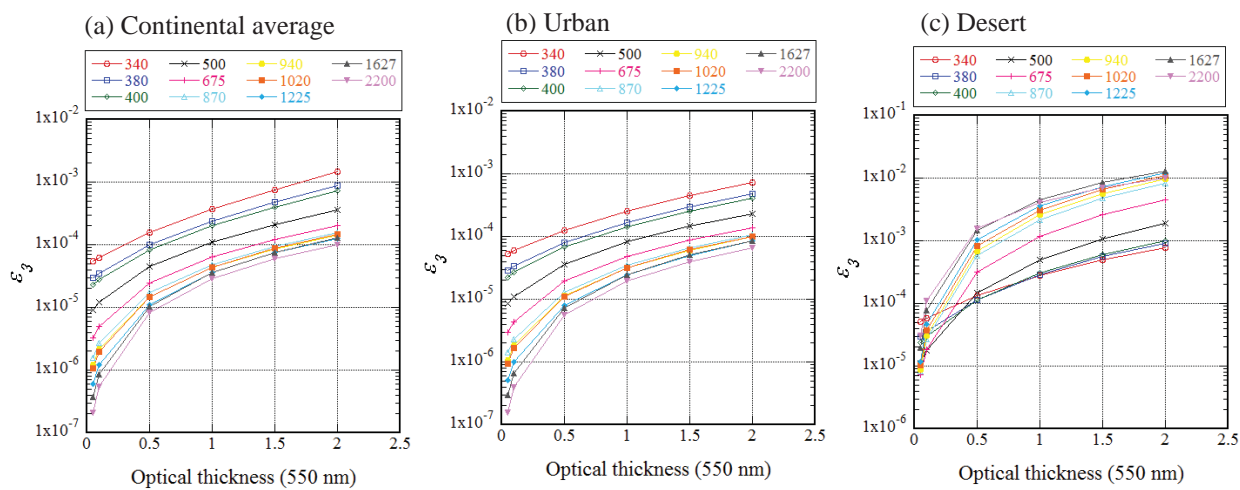


Fig. 3 Same as Fig. 2 but for error  $\varepsilon_3$ .



Fig.4

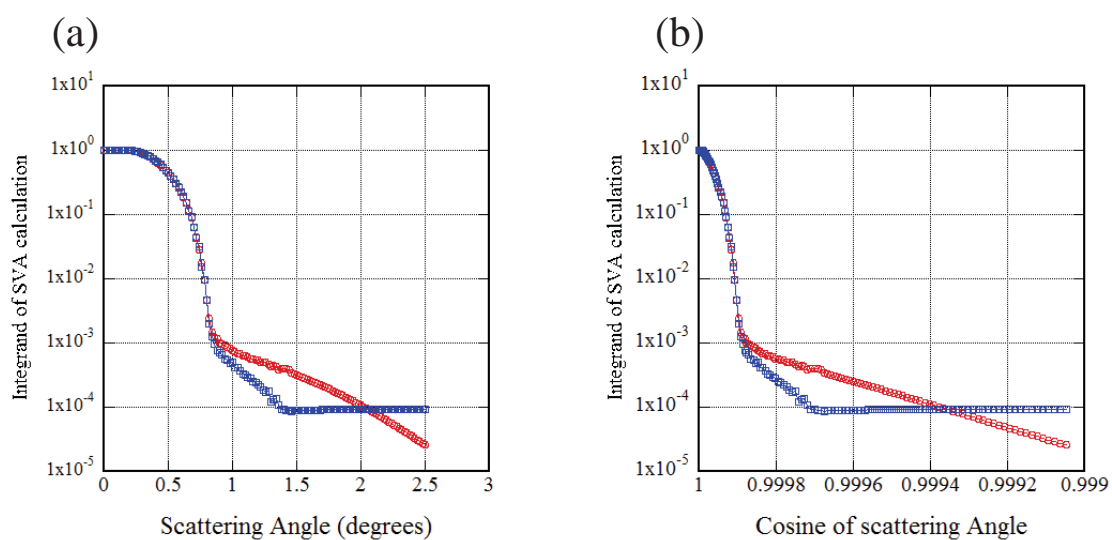


Fig.4 An example of integrand of SVA calculation. The blue line with open squares is the case that the minimum value is subtracted, and the red line is the case that the values between 1.4 and 2.5 degrees are extrapolated using the data from 1.0 to 1.4 degrees

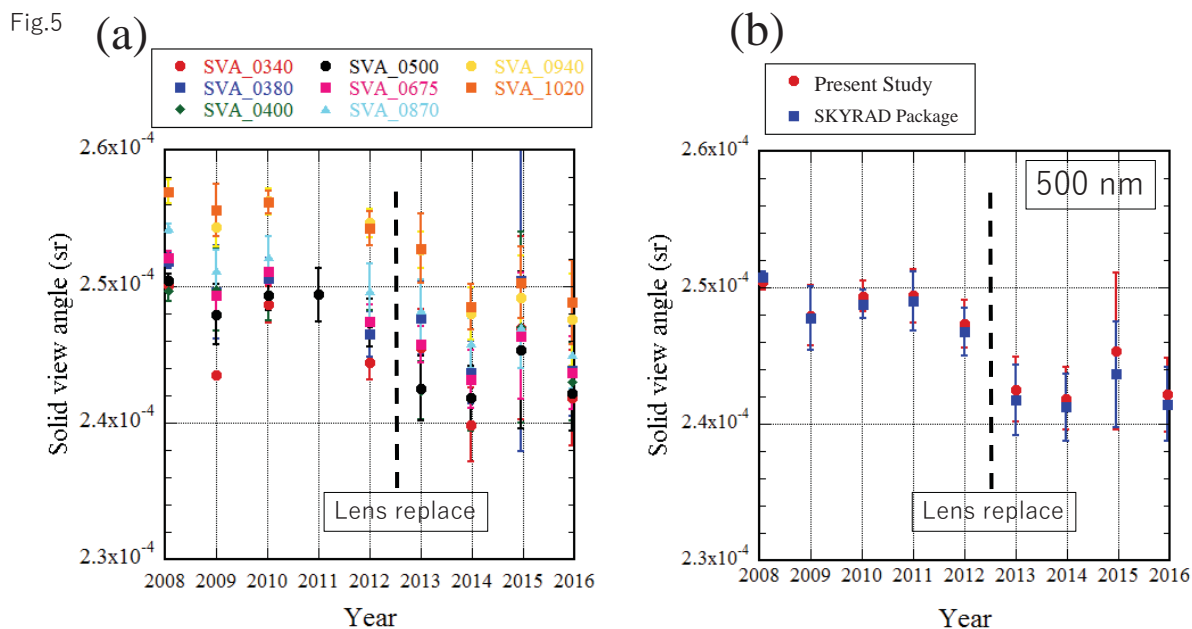


Fig.5 SVAs in the visible region (Si photodiode) from 2008 to 2016. The data were taken at MLO during about a month in October and November every year. (a) SVA calculated by the corrected method in this study, (b) SVA at the wavelength of 500 nm calculated by both the corrected and the current SKYRAD package methods.

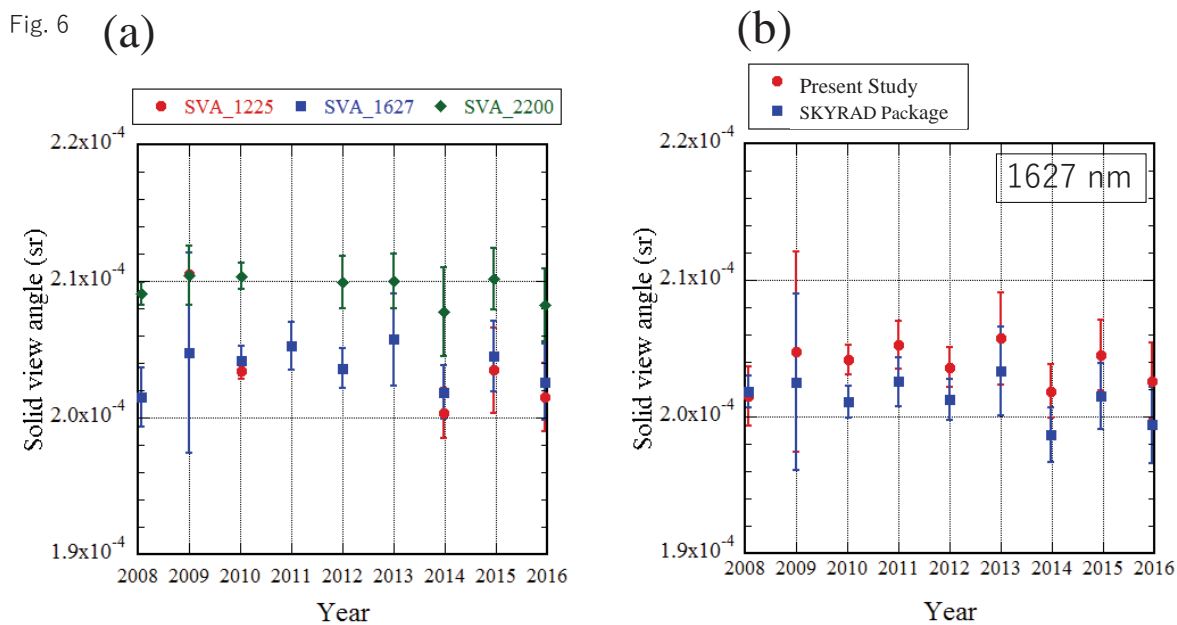


Fig.6 Same as Fig. 5 but for the near infrared region (InGaAs photodiode). The wavelength in (b) is 1627 nm.



Fig. 7

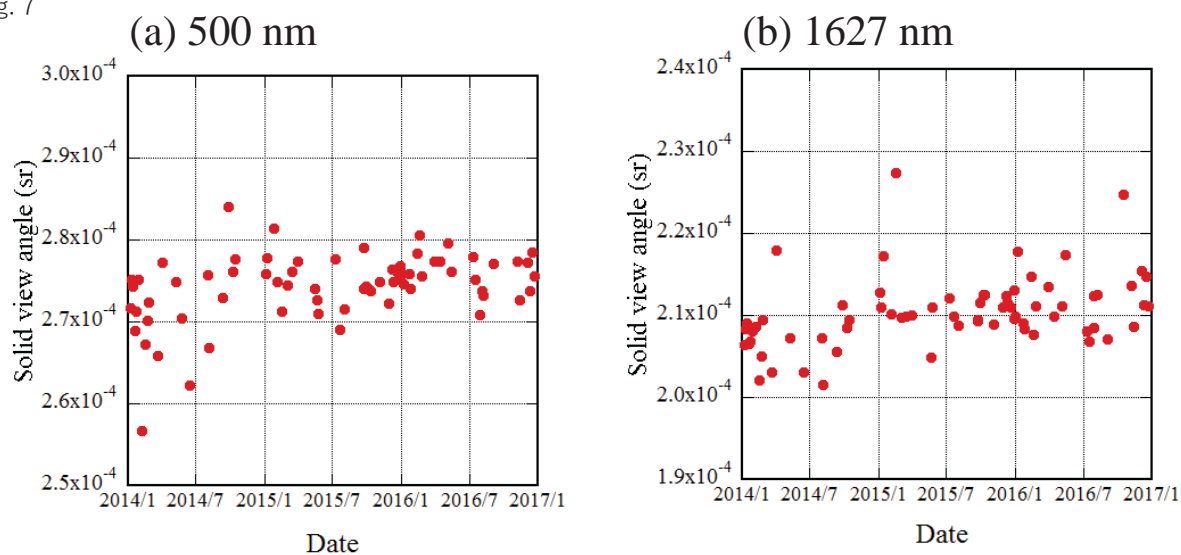


Fig.7 Time series of SVA of POM-02(Tsukuba) in the period from January 2014 to December 2016, (a) 500nm, (b) 1627nm.